DOI: 10.1002/ejoc.200600133

Chiral C_2-Boron-Bis(oxazolines) in Asymmetric Catalysis – A Theoretical Study of the Catalyzed Enantioselective Reduction of Ketones Promoted by Catecholborane

Marco Bandini,[a] Andrea Bottoni,[a] Pier Giorgio Cozzi,[a] Gian Pietro Miscione,*[a] Magda Monari,[a] Rossana Pierciaccante,[a] and Achille Umani-Ronchi[a]

Keywords: Ab initio calculations / Reaction mechanism / Asymmetric catalysis / Reduction / Boron-bis(oxazolines)

C_2-Symmetrical boron complexes, prepared by the reactions of 2,2′-methylenebis(oxazolines) (BOXs) with catecholborane (CATBH), can be used as catalysts (5–10 mol-%) in the enantioselective reduction of prochiral ketones (*ee* 72–86 %), giving the desired alcohols in satisfactory yields. We have theoretically investigated the mechanism of the reduction of chloroacetophenone at the DFT level and the computational results have provided a complete mechanistic picture, which explains the stereochemical outcome of the reaction. The B–BOXate complex binds both the reducing agent CATBH and the carbonyl compound, activating the former as a hydride donor and enhancing the electrophilicity of the latter. Moreover, the structure of two boron–BOX (BOXate) complexes has been confirmed by means of X-ray diffraction techniques.

(© Wiley-VCH Verlag GmbH & Co. KGaA, 69451 Weinheim, Germany, 2006)

Introduction

Chiral bis(oxazoline) (BOX) species are considered "privileged ligands"[1] and have been used in many catalyzed stereo-controlled reactions.[2] Chiral Lewis acids are usually obtained from bis(oxazolines) and an appropriate metal with free coordination sites. The role of the metal is to activate electrophiles towards the attack of nucleophiles or masked enolates.[3] C_2-Bis(oxazolines) bearing a methylene bridge between the two dihydrooxazole rings can be easily deprotonated and several research groups have been able to functionalize this type of ligand (Scheme 1) by introducing carbon chains with different functions and to anchor the BOX species to solid supports[4] or to soluble polymers.[5] Furthermore, the organometallic chemistry of metallated bis(oxazolines) has been described in several papers.[6] Hoffmann, for instance, has reported the preparation of magnesium–BOX compounds[7] (Scheme 1, M = Mg), while Zn–BOX complexes have been synthesized by Nakamura[8] and Singh.[9] Quite recently our group has described the preparation of Ti–BOX complexes and their use in catalytic enantioselective reduction of ketones. In this case the whole catalytic cycle has also been theoretically investigated at the DFT level.[10]

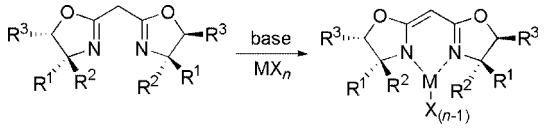

Scheme 1.

The main BOX skeleton is identical to that of β-diketiminate (Figure 1), which has been known for a long time and was initially employed in the spectroscopic studies of coordination compounds.[11] In addition to many applications of monoanionic β-diketiminates in coordination chemistry,[12] Smith III and co-workers[13] have recently reported an interesting study of the structure and properties of β-diketiminate boron complexes. The similarity between BOX and β-diketiminate framework, the structural features of β-diketiminate boron compounds and their stability, has prompted us to consider the possibility of designing boron–BOX complexes to be used in catalytic enantioselective reactions. As a result of our research, we have discovered that achiral and chiral BOX compounds react with catecholborane affording a stable boron-bis(oxazolinate) adduct and that chiral bis(oxazolines) are able, in the presence of CATBH, to reduce pro-chiral ketones with good enantioselectivity.[14,15]

In this paper, in order to elucidate the mechanism of this reaction and to understand the reasons for the aforementioned stereoselectivity, we have carried out a theoretical investigation of the whole catalytic cycle at the Density Functional Theory (DFT) level. To this purpose, we have used a model system consisting of one chiral boron–BOX complex, one molecule emulating the CATBH and a chlo-

[a] Dipartimento di Chimica "G. Ciamician", Università di Bologna,
Via Selmi 2, 40126 Bologna, Italy
Fax: +39-051-2099456
E-mail: gianpietro.miscione@unibo.it

Supporting information for this article is available on the WWW under http://www.eurjoc.org or from the author.

 © 2006 Wiley-VCH Verlag GmbH & Co. KGaA, Weinheim

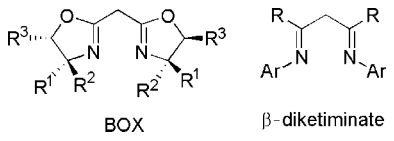

Figure 1. BOX and β-diketiminate. The two species have similar skeletons.

roacetophenone molecule as the substrate. Although several important computational studies have been carried out on similar catalytic systems,[16] as far as we know, no theoretical investigations on this specific subject can be found in the literature. We also report details and information about the structure of the chiral boron–BOX complex obtained from X-ray diffraction techniques.

Results and Discussion

A. Experimental Results

To prepare coordinatively saturated boron-bis(oxazolinate) complexes, the reaction of achiral BOX **1** (Scheme 2) with catecholborane was carried out in CH_2Cl_2 for 24 h at room temperature. A white solid, stable to moisture and oxygen, was isolated after removal of the solvent. The ^1H, ^{13}C and ^{11}B NMR spectroscopic investigations supported the hypothesis for the formation of a single complex derived from the reaction of CATBH with BOX **1** (boron–BOXate). The reaction is quite general and the synthesis of other boron–BOXate species was also readily accomplished from chiral bis(oxazolines). In this way, the boron–BOXate complexes **4**–**6** (from **1**, **2** and **3**, respectively) were prepared and isolated in good yields, monitoring the deprotonation process at the methylene bridge by NMR spectroscopy. The diagnostic NMR signals for the boron–BOXate complexes derived from the achiral bis(oxazoline) **1** are the singlet for the proton bridge at δ = 4.45 ppm and the corresponding ^{13}C NMR signal at δ = 57.8 ppm, both characteristic of methine carbons. On the other hand, the ^{11}B NMR signal at δ = 8.87 ppm represents a typical value for a tetrahedral coordination at the boron atom. Recently, borates derived by the reaction between the reaction of (1*R*,2*S*)-norephedrine and diphenylprolinol with catecholborane were characterized[17] by ^{11}B NMR, the characteristic signals for the central atom were observed at δ = 11.6 and 11.7 ppm, respectively.

The X-ray diffraction study carried out on **4** and **6** is consistent with the NMR interpretation. The ORTEP plots with the two structures are depicted in Figure 2 and Figure 3 whereas the relative values obtained for selected bond lengths and angles are collated in Table 1. The two molecules conform to an idealized C_2-symmetry with the boron atom exhibiting a slightly distorted tetrahedral geometry upon coordination of a chelating bis(oxazolinate) ligand and a chelating catecholate unit. The BOX and catecholate ligands lie on almost perpendicular planes [the dihedral angle between the N1–B1–N2 and O3–B1–O4 planes is 89.69 (8)° and 87.7 (1)° in **4** and **6**, respectively]. The boron atom is coplanar with the catecholate ring in **4** but "tipped" out of the plane by ca. 0.15 Å in compound **6**, presumably because of crystal packing forces. The six-membered rings, formed by coordination of the two nitrogen atoms of the bis(oxazolinate) ligand to the boron, show some deviation from planarity. The negative charge of the bis(oxazolinate) ligand is delocalized, as clearly indicated by the C–C and C–N bond interactions [C4–C5 1.370 Å and C4–C3 1.375(2) Å; N1–C3 1.316 Å and N2–C5 1.1.319(2) Å in **4**; C11–C10 1.382 Å and C11–C27 1.371(3) Å; N1–C10 1.332 Å and N2–C27 1.319(2) Å in **6**]. Interestingly, the N–B–N bite angle [105.8° and 105.2(1)° in **4** and **6**, respectively] is rather large when compared to the bite angles in related tetrahedral metal complexes containing the chelating bis(oxazolinate) ligand. For example, the N–Metal–N bite angle of the metallacycle is 93.13(7)° in (BOX-Me_2)$AlMe_2$ and 97.35(8)° in (BOX-Me_2)$AlCl_2$[18] and as narrow as 85.2(1)° in the [(4*S*)*i*BuBox]Lu[$CH(TMS)_2$]$_2$ complex.[19] This rather wide range of values demonstrates the high flexibility of the bis(oxazolinate) ligand.

Achiral and chiral boron complexes **4**–**6** were able to reduce pro-chiral ketones with good enantioselectivity, employing CATBH as the reducing agent, as shown in Scheme 3.[14] The corresponding results (yields and enantiomeric excesses) are reported in Table 2.

On the basis of the experimental evidence, it turned out to be very difficult to propose a plausible reaction mechanism: the saturated boron coordination spheres in these B–

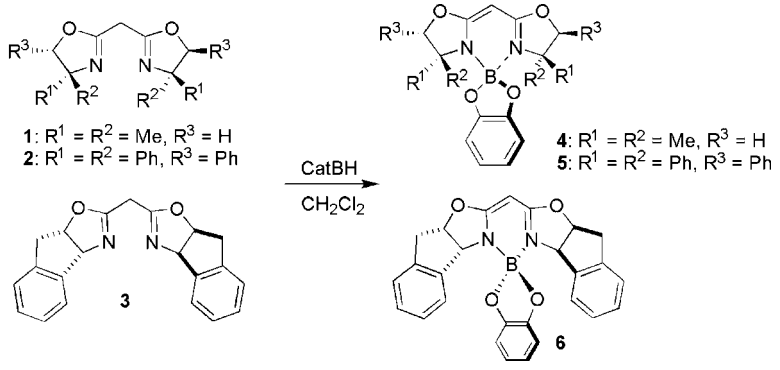

Scheme 2.

 © 2006 Wiley-VCH Verlag GmbH & Co. KGaA, Weinheim

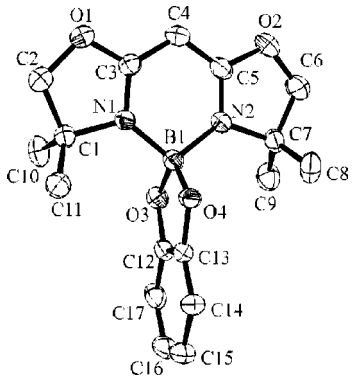

Figure 2. ORTEP drawing for compound **4**. The hydrogen atoms are omitted for clarity.

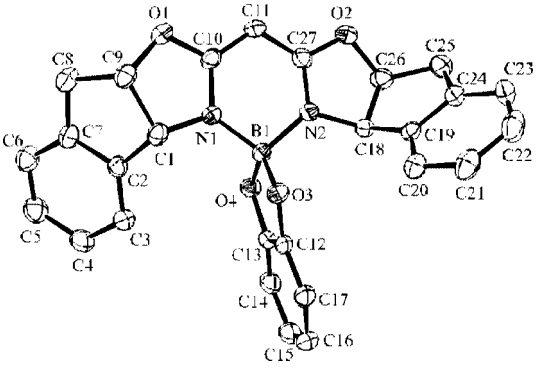

Figure 3. ORTEP drawing for compound **6**. The hydrogen atoms are omitted for clarity.

Table 1. Selected bond lengths [Å] and angles (°) for compounds **4** and **6** obtained in the X-ray diffraction study. The values in the brackets refer to the error in the measurement. It can be noted that the data are quite accurate. For comparison, the geometrical parameters obtained computationally for the isolated BOX-ate (which is more similar to 6, see Figure 5) have been included.

	Compound **4**	Compound **6**	Computational results
B1–N1	1.541(2)	1.525(2)	1.548
B1–N2	1.548(2)	1.544(2)	1.551
B1–O3	1.481(2)	1.472(2)	1.482
B1–O4	1.479(2)	1.484(2)	1.478
N1–C3	1.316(2)	–	
N2–C5	1.319(2)	–	
C3–C4	1.375(2)	–	
C4–C5	1.370(2)	–	
N1–C10	–	1.332(2)	1.335
N2–C27	–	1.319(2)	1.334
C10–C11	–	1.382(3)	1.391
C11–C27	–	1.371(3)	1.390
O3–B1–O4	104.5(1)	104.8(1)	104.9
N1–B1–N2	105.8(1)	105.2(1)	104.1
C5–C4–C3	115.7(2)	–	
C10–C11–C27	–	115.6(2)	115.7
N1–B1–O3	111.3(1)	111.8(2)	111.7
N2–B1–O3	111.9(1)	112.7(2)	111.8
N1–B1–O4	111.8(1)	113.9(2)	112.8
N2–B1–O4	111.6(1)	108.6(2)	111.7

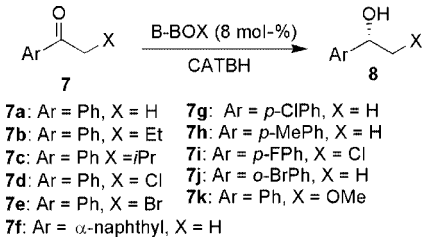

Scheme 3.

Table 2. Yields and the enantiomeric excesses obtained with various ketones.

Entry	Ketone	Yield (%)	*ee* (%)
1	**7a**	80	76 (*R*)
2	**7b**	65	76 (*R*)
3	**7c**	57	74(*R*)
4	**7d**	85	84 (*S*)
5	**7e**	54	86 (*S*)
6	**7f**	78	72 (*R*)
7	**7g**	72	74 (*R*)
8	**7h**	65	74 (*R*)
9	**7i**	67	81 (*S*)
10	**7j**	55	57 (*R*)
11	**7k**	42	58 (*R*)

BOXate complexes do not imply trivial mechanistic explanations. Thus, in order to obtain detailed information about the process of the reaction, with particular regard to the stereochemical aspects and to understand the role played by the B–BOXate, we have examined the mechanism of the process at a theoretical level, using a DFT approach. The results are reported in the following section.

B. Computational Results: The Choice of the Model

The model system, represented in Figure 4, was chosen as it closely resembles the real molecules involved in the reaction. Also, the two basis sets used in the computations are indicated in the Figure: the DZVP basis for the atoms directly involved in the reaction and the 3-21G* basis set for the remaining atoms (see the Computational Details section). This system includes a chloroacetophenone molecule (substrate, corresponding to entry **7d** in Scheme 3), one molecule emulating the catecholborane (CATBH) and a chiral catalytic B–BOXate species, which mimics compound **6** (obtained from **3**) of Scheme 2. In the real complex, which is characterized by an inversion center, a benzene ring is bound to each of the two five-membered cycles, pointing above and under the BOX plane. To avoid heavy computations, we have reduced the size of the B–BOXate and we have considered only one of these cycles. Furthermore, we have replaced the benzene ring fused with this cycle with a C=C double bond and we have used the same approximation to simplify the catecholborane molecule. Thus, a penta-atomic unsaturated ring, approximately orthogonal to the BOX plane, characterizes the resulting B–BOXate complex.

 © 2006 Wiley-VCH Verlag GmbH & Co. KGaA, Weinheim

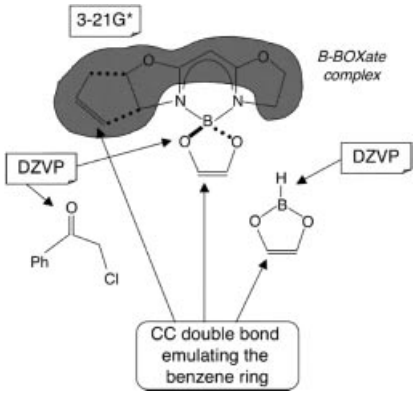

Figure 4. The model system used to investigate the mechanism of the catalyzed ketone reduction. The different basis sets used in the various molecular regions are indicated.

This B–BOXate complex, although being different from the real system, is chiral and can be successfully used to obtain information on the stereochemical outcome of the reaction. This is possible in a theoretical study, by making the reaction take place in the desired position: in the present case this has been achieved by placing the reducing agent and the substrate under the B–BOXate plane, as shown in Figure 5, in such a way as to let them interact with the unsaturated cycle. Of course, under the real experimental conditions, the reaction can take place on both sides of the molecular plane. Thus, by forcing the reaction to occur on one side of the plane only, where the chirality elements are placed, we can use the present system as a reliable model of the real one, without adding the second five-membered ring.

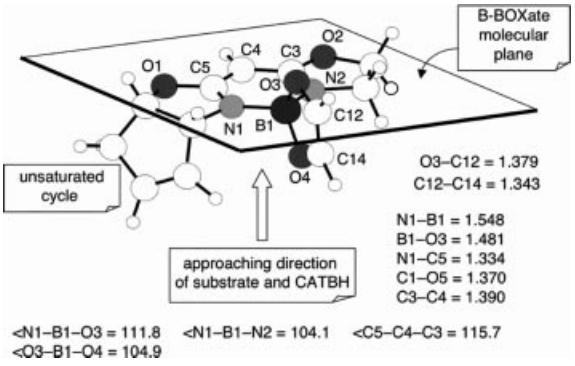

Figure 5. A schematic representation of the direction of attack of the substrate and CATBH with respect to the B–BOXate molecular plane. The values of selected geometrical parameters (Å and °) are reported.

It is interesting to compare the values of some selected geometrical parameters computed at the DFT level for the model B–BOXate complex to the corresponding values obtained in the X-ray diffraction study for compounds **4** and **6** (see Table 1). The agreement between the two sets of values is very satisfactory. This result indicates that the computational level used here is adequate to provide a reliable description of the system.

C. Computational Results: The Reaction Mechanism

In this section we discuss in details the singlet potential energy surface associated with the various steps of the reaction. The corresponding mechanistic scheme is illustrated in Scheme 4. A representation of the energy profile is given in Figure 6, while the structures of the various critical points located along it are shown in Figure 7, Figure 8, Figure 9, Figure 10 and Figure 11. In Figure 6, the energy values obtained with single-point calculations with the DZVP basis set on all atoms are also reported in square brackets. The reaction sequence reported at the bottom of Figure 6 corresponds to the mechanistic steps of Scheme 4.

A preliminary encounter complex (long-range complex **M1** in Figure 7), involving the B–BOXate, the CATBH molecule and the substrate, is found in the first reaction step. Formation of **I** does not require any activation barrier. In this complex, which is 7.0 kcal mol^{-1} more stable than the reactants (asymptotic limit), the carbonyl bond of the substrate interacts with the B–BOXate system through a hydrogen bond with the bridging CH group of the central B–BOXate ring (O5–H distance 2.476 Å). A second interaction that contributes to stabilize the complex involves the catecholborane boron atom B2 and the B–BOXate oxygen O4, the B2–O4 distance being 2.803 Å.

The next step of the catalytic cycle (**I**→**II**) is the ketone reduction and represents the rate-determining step of the process. Several transformations take place to allow the hydride transfer. The O4–B1 bond is replaced by the O4–B2 bond, which determines the opening of the catecholborane ring of the B–BOXate system. This makes the boron atom (electronically saturated and sterically hindered in **M1**) available for the interaction with the ketone acting as a Lewis base. In this new arrangement, the boron atom B1 adopts a trigonal coordination state. Furthermore, the conjugation of the O4 lone pair with the LUMO of B2 shifts the electron density along the B1–O3–C12–C13–O4–B2–H chain and has the effect of making B1 more electrophilic and the hydride more nucleophilic. In spite of extensive search it was not possible to locate any critical point preceding the reduction and corresponding to the previously described transformations (breaking of the O4–B1 and formation of O4–B2 bonds). Our investigation has shown that this region of the potential energy surface is very flat indeed.

During the ketone reduction a hydride ion is transferred from the boron atom B2 to the prochiral carbon C14 leading to a new chiral center. It is evident that, because of the presence of the five-membered unsaturated cycle in the B–BOXate catalytic complex, the probabilities for the attack of the hydride ion on the two faces of the carbonyl group are not the same. The reduction can occur along two different channels involving two different diastereotopic transition states: **TS1(S)** and **TS1(R)** (Figure 8 and Figure 9, respectively). **TS1(S)** describes the transfer of the hydride onto the *Re* face of the ketone. In this structure, the new forming C14–H bond is 2.071 Å, while the breaking B2–H bond is 1.256 Å. This transition state is 22.7 kcal mol^{-1}

 © 2006 Wiley-VCH Verlag GmbH & Co. KGaA, Weinheim

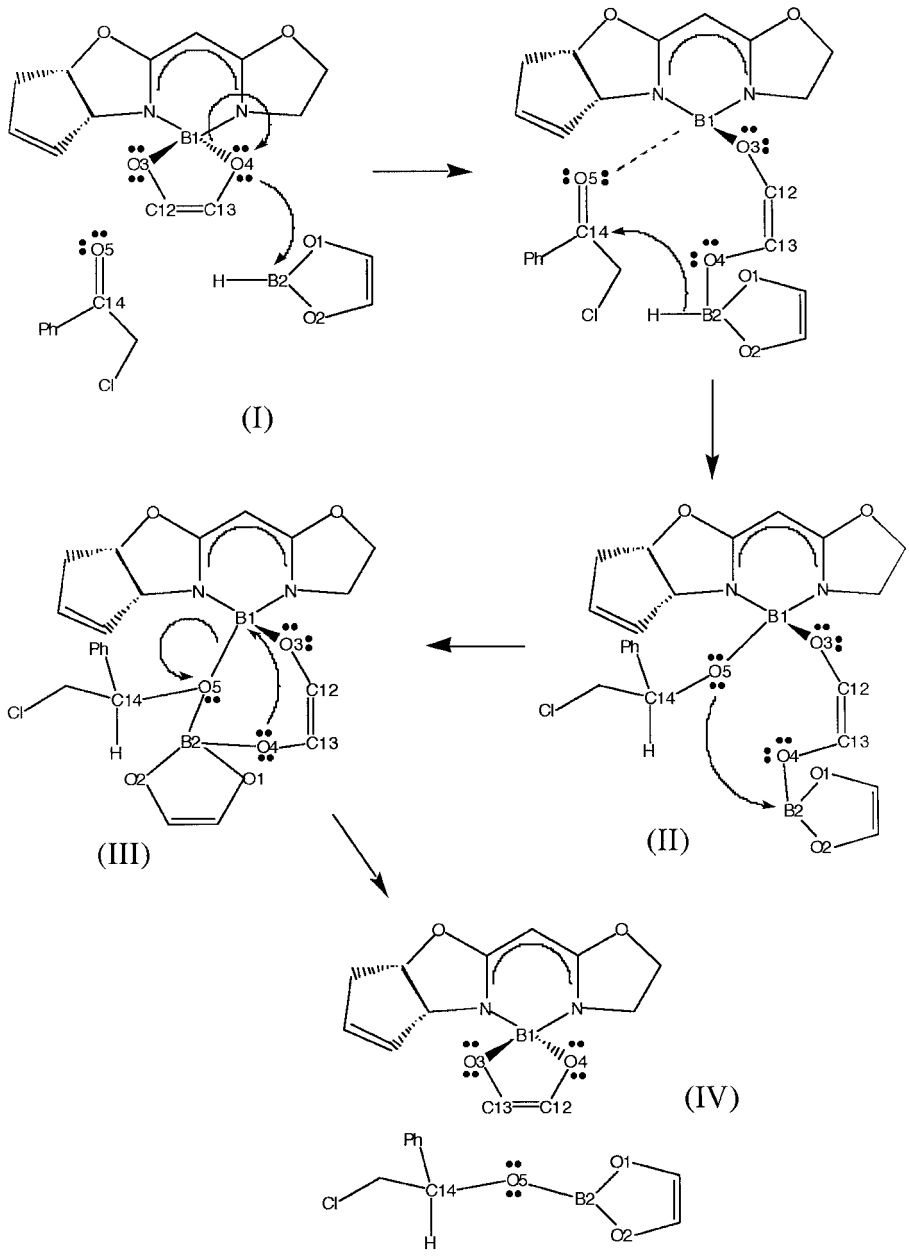

Scheme 4. The reaction mechanism.

above the reactants and leads to configuration *S* at the new chiral center. **TS1(R)** (transfer of the hydride onto the *Si* face; C14–H 1.542 Å and B2–H 1.335 Å), leading to configuration *R*, is significantly higher in energy (by 4.3 kcal mol^{-1}). Since this is the key step for determining the stereochemical outcome of the reaction and is also clearly irreversible, the formation of the stereoisomer with configuration *S* at C14 is highly favored in agreement with the experimental evidence. The lower energy of **TS1(S)** with respect to **TS1(R)** is partly due to the stabilizing B1–O5 interaction (acid–base interaction), which is considerably stronger in the former case than in the latter [the B1–O5 distance is 1.901 Å in **TS1(S)** and becomes 2.392 Å in **TS1(R)**]. This interaction certainly makes the C14 carbon more electrophilic in **TS1(S)** than in **TS1(R)** and makes the nucleophilic attack of the hydride ion easier.

The key factors that prevent the ketone carbonyl group from getting close enough to the B1 atom in **TS1(R)** are the steric interactions between the ketone substituents and the B–BOXate system and the repulsion between the O5 and O4 oxygen atoms. This repulsion is certainly lower in **TS1(S)** than in **TS1(R)** since the O5–O4 distance is 2.940 Å in the former case and 2.893 Å in the latter. In **TS1(S)**, the carbonyl group of the ketone can get closer to B1 and increase the stabilizing acid–base interaction (without making the O5–O4 interaction too strong), by decreasing the B1–

 © 2006 Wiley-VCH Verlag GmbH & Co. KGaA, Weinheim

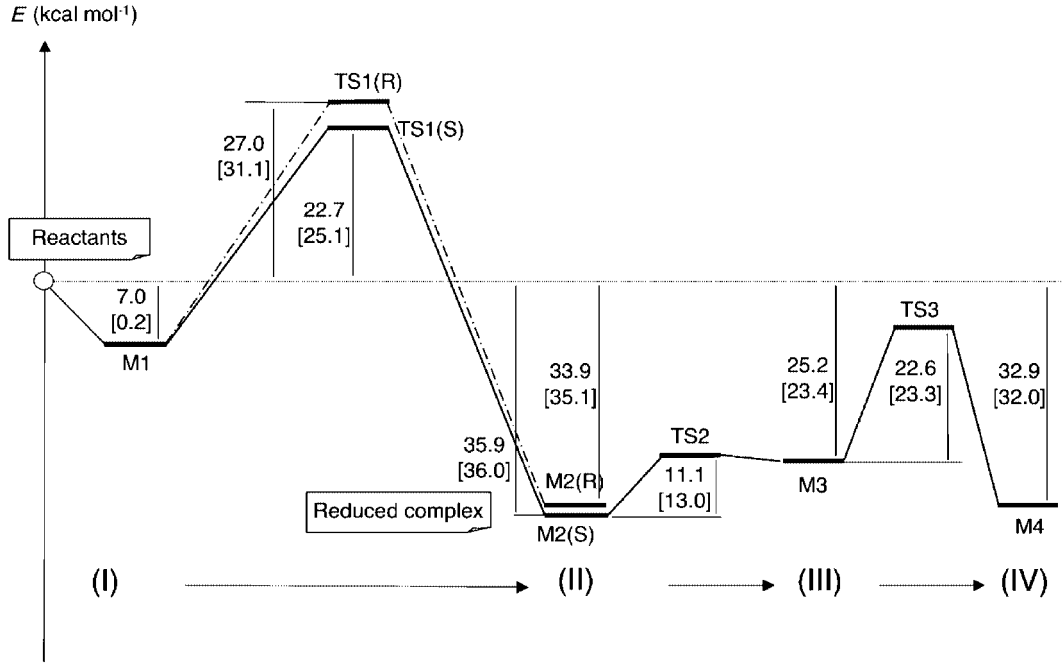

Figure 6. Total energy profile for the whole catalytic cycle corresponding to the reduction of chloroacetophenone. The energy values include the ZPE corrections. In square brackets, energy values obtained with single-point calculations with DZVP basis on all atoms.

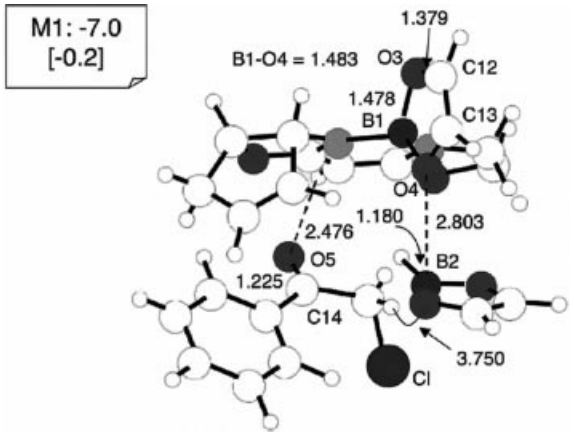

Figure 7. Schematic representation of the structure of the critical point **M1**. The total energy value (kcal mol^{-1}) relative to reactants (B–BOXate + CATBH + chloroacetophenone) and some selected geometrical parameters (Å) are reported. The energy values include the ZPE corrections. In square brackets, energy values obtained with single-point calculations with DZVP basis on all atoms.

O5–C14 angle that becomes 147.2°. More precisely, as the ketone approaches the catalyst, it can slightly bend with respect to an ideal straight line of attack (B1–O5–C14 180°) to minimize the repulsive steric interactions of its substituent with the catalyst. A similar distortion of the B1, O5, C14 system is not possible in **TS1(R)** (here the B1–O5–C14 angle is larger i.e. 154.8°) since in this case it would firstly cause an enhancement of the steric repulsion between the unsaturated ring of the B–BOXate and the CH_2Cl group.

In Figure 9 we have reported the distances between the two hydrogen atoms of the methylene group and the closest hydrogen of the B–BOXate unsaturated ring in **TS1(R)**. These distances are 2.537 and 3.028 Å, respectively. It is interesting to point out that a rotation around the C–C14 bond could not help to reduce the repulsion, since a decrease of one H···H distance after rotation, is necessarily accompanied by an increase of the other H···H distance. Things are different in **TS1(S)**, where the planar phenyl ring, by rotating around the C(phenyl)–C(carbonyl) bond, can easily find the best orientation to minimize the repulsion that involves one H···H pair of atoms (see Figure 8) only. In the end, the position of the ketone (and thus the magnitude of the stabilizing O5–B1 interaction and the different stability of the two transition states) is the result of a complex interplay between the O5–O4 repulsion and the repulsion involving the ketone substituents and the unsaturated five-membered B–BOXate cycle.

The free-energy difference between **TS1(R)** and **TS1(S)** is 4.4 kcal mol^{-1} and thus, almost identical to the total energy difference. This value would correspond to an enantiomeric excess above 99%, and thus, does not exactly predict the experimental outcome (corresponding to an enantiomeric excess of about 80%). However, it provides the correct indication of the stereochemical preference of the reaction, in agreement with the experimental evidence.

It can be argued that the relative position of the two reactants (catecholborane including the reducing hydride and ketone) may be interchanged with respect to the five-membered cycle of the BOX system (i.e the ketone may be placed far from it, on the right side, according to the orientation of the figures). The transition states for this alternative arrangement have been calculated. Actually, these points [**TS1(S)′** and **TS1(R)′** reported in the Supporting Information] are almost degenerate to **TS1(S)** and **TS1(R)**, respectively, indicating that this different approach is ener-

 © 2006 Wiley-VCH Verlag GmbH & Co. KGaA, Weinheim

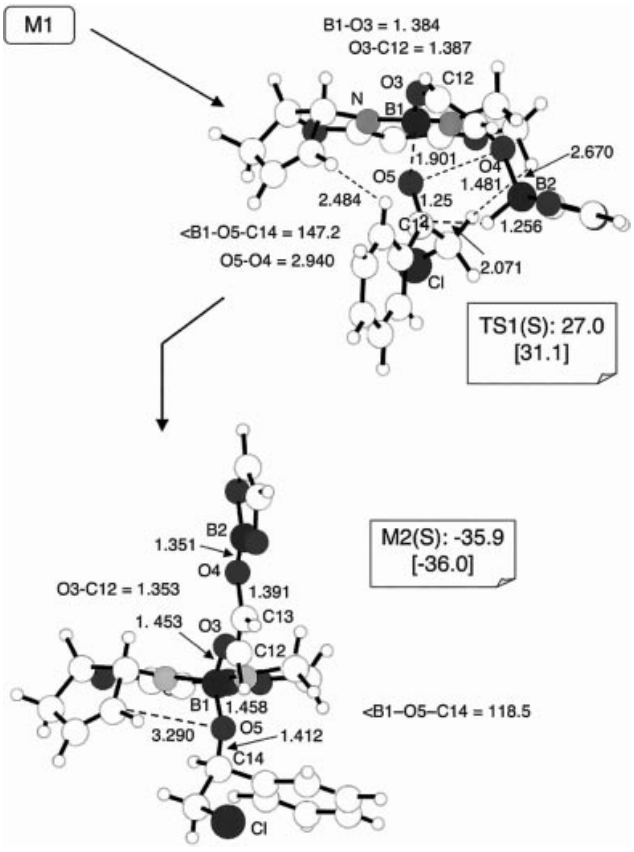

Figure 8. Schematic representation of the structure of the critical points **TS1(S)** and **M2(S)**. The total energy value (kcal mol^{-1}) relative to reactants (B–BOXate + CATBH + chloroacetophenone) and some selected geometrical parameters (Å) are reported. The energy values include the ZPE corrections. In square brackets, energy values obtained with single-point calculations with DZVP basis on all atoms.

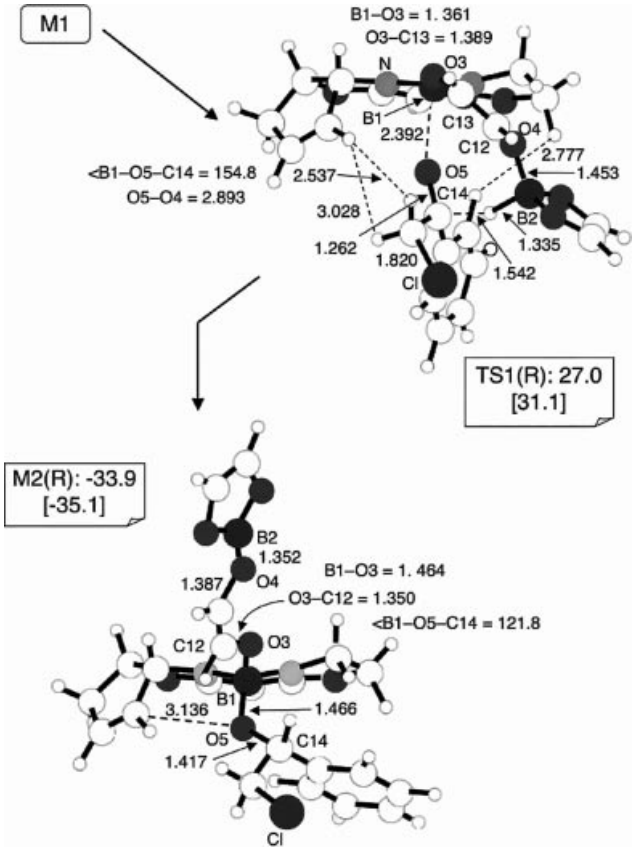

Figure 9. Schematic representation of the structure of the critical points **TS1(R)** and **M2(R)**. The total energy value (kcal mol^{-1}) relative to reactants (B–BOXate + CATBH + chloroacetophenone) and some selected geometrical parameters (Å) are reported. The energy values include the ZPE corrections. In square brackets, energy values obtained with single-point calculations with DZVP basis on all atoms.

getically equivalent to that originally considered. Thus, even in this case a preference for the path leading to the stereoisomer with *S* configuration at C14 is still observed [the total energy difference and the free-energy difference between **TS1(S)′** and **TS1(R)′** are 2.8 kcal mol^{-1} and 3.2 kcal mol^{-1}, respectively].

The two transition states **TS1(S)** and **TS1(R)** lead to two diastereomeric reduced species [**M2(S)** and **M2(R)**, respectively], both corresponding to an oxaborane bound to the B–BOXate system and differing only for the configuration at C14. The two complexes (see Figure 8 and Figure 9), where B1 has a tetrahedral coordination, feature the "unfolding" of the two chains bound to B1, one above and the other under the N–B1–N plane. The groups bound to C14 (new chiral center) are oriented in such a way that the phenyl substituent approximately points in the opposite direction with respect to the five-membered ring. Both species are very stable: **M2(S)** and **M2(R)** are 35.9 and 33.9 kcal mol^{-1} lower than the asymptotic limit, respectively. This indicates that the transfer of the hydride is a highly exothermic process. Because of the different configuration at the chiral center C14, the oxygen atom O5 in **M2(R)** is closer to the unsaturated five-membered cycle than in **M2(S)** [the O5–C(ring) distance is 3.290 and 3.136 Å in **M2(S)** and **M2(R)**, respectively]. Furthermore, in **M2(R)** the O3–C12–C13–O4–B2 chain is oriented toward the ring and this causes an increase of the hydrogen C12–hydrogen(ring) interaction. These structural features have the effect of making **M2(S)** more stable than **M2(R)**.

Since the results of the calculations indicate that **M2(S)** is the most likely reaction product, in agreement with the experimental outcomes (the stereoisomer with *S* configuration at C14 is formed in 84% *ee*[14]), from now on, only the remaining path related to this isomer will be discussed. This path, corresponding to the closure of the catalytic cycle (regeneration of the catalyst and release of the oxaborane), is accomplished in two steps: **II**→**III** [corresponding to the **M2(S)**→**TS2**→**M3** transformation] and **III**→**IV** (corresponding to the **M3**→**TS3**→**M4** transformation).

In **TS2** (see Figure 10), the O3–C12–C13–O4–B2 chain is folded down to form the new B2–O5 bond. The transition state has a strong product-like character with the boron-oxygen bond almost completely formed (the B2–O5 distance is 1.811 Å). This structural change, which entails a change of the B2 coordination state (from tri-coordinated to tetra-coordinated), results in a lengthening of the B1–O5

 © 2006 Wiley-VCH Verlag GmbH & Co. KGaA, Weinheim

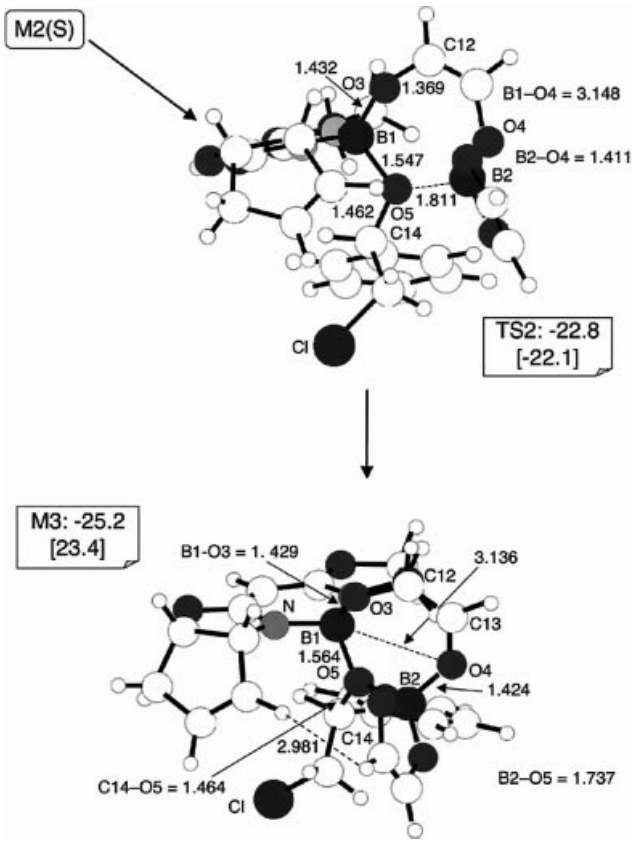

Figure 10. Schematic representation of the structure of the critical points **TS2** and **M3**. The total energy value (kcal mol^{-1}) relative to reactants (B–BOXate + CATBH + chloroacetophenone) and some selected geometrical parameters (Å) are reported. The energy values include the ZPE corrections. In square brackets, energy values obtained with single-point calculations with DZVP basis on all atoms.

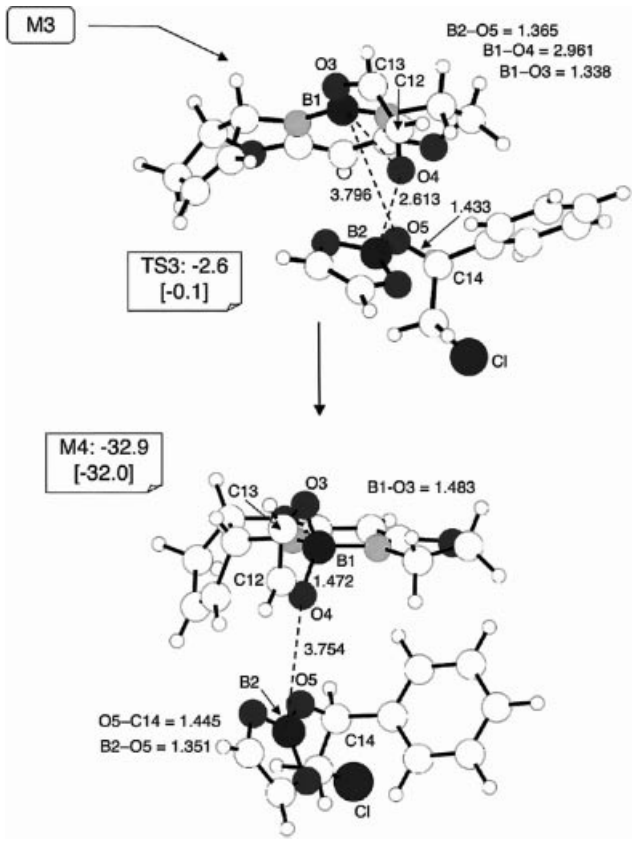

Figure 11. Schematic representation of the structure of the critical points **TS3** and **M4**. The total energy value (kcal mol^{-1}) relative to reactants (B–BOXate + CATBH + chloroacetophenone) and some selected geometrical parameters (Å) are reported. The energy values include the ZPE corrections. In square brackets, energy values obtained with single-point calculations with DZVP basis on all atoms.

and B2–O4 bonds that become 1.547 and 1.411 Å, respectively. The barrier required by this transformation is 11.1 kcal mol^{-1} and probably, is mainly caused by the B1–O5 and B2–O4 lengthening and by the steric effect of the penta-atomic cycle bonded to O4. The resulting intermediate **M3** (Figure 10) is characterized by a seven-member cycle that includes the O5 oxygen bonded to the chiral C14 carbon. **M3** is 10.7 kcal mol^{-1} higher than **M2(S)** and 25.2 kcal mol^{-1} below the asymptotic limit. This energy increase is certainly caused by the proximity of the CATBH ring to the unsaturated penta-atomic cycle.

To close the catalytic cycle the breaking of two boron-oxygen bonds (B2–O4 and B1–O5) and the formation of a new boron-oxygen bond (B1–O4) must take place. This transformation can be accomplished in one step (step **III**→**IV**): release of the oxaborane and regeneration of the catalyst by overcoming a barrier of 22.6 kcal mol^{-1}. In the corresponding transition state **TS3** (see Figure 11), the two breaking bonds B2–O4 and B1–O5 are 2.613 and 3.796 Å, respectively. The B1–O3–C13–C12–O4 chain is simultaneously folded down to form the new bond B1–O4, which is still far from being completed (B1–O4 2.961 Å). The reaction is highly exothermic, the final complex **M4** (Figure 11) being 32.9 kcal mol^{-1} lower than reactants. In **M4** the B1–O3–C13–C12–O4 cycle of the regenerated catalyst is completed with the two B1–O3 and B1–O4 bonds almost equivalent (1.483 and 1.472 Å, respectively). The product molecule is still slightly interacting with the catalyst, the B2–O4 distance being 3.754 Å.

Further calculations have been carried on a more realistic model system that includes the phenyl group attached to the five-membered cycle. In these calculations we have considered either the two transition states where the ketone is close to the five-membered ring and the phenyl group [**TS1-phen(S)** and **TS1-phen(R)**, see Figure 12] and those corresponding to the opposite arrangement [**TS1-phen(S)′** and **TS1-phen(R)′**, see Supporting Information]. The results have confirmed the following important aspects: (i) the already observed arrangement of the two reactants in **TS1(S)** and **TS1(R)**, i.e. the ketone near to the five-membered ring, is favored [**TS1-phen(S)** is 1.8 kcal mol^{-1} more stable than **TS1-phen(S)′**, whereas **TS1-phen(R)** is 4.4 kcal mol^{-1} below **TS1-phen(R)′**]. The corresponding free-energy values are 1.2 kcal mol^{-1} and 2.6 kcal mol^{-1}, respectively: (ii) a significant preference for the path leading to the *S* stereoisomer is once again observed. The total energy and free-energy

 © 2006 Wiley-VCH Verlag GmbH & Co. KGaA, Weinheim

differences between **TS1-phen(S)** and **TS1-phen(R)** are 1.1 kcal mol^{-1} and 0.9 kcal mol^{-1}, respectively. It is interesting to underline that this free-energy difference would correspond to an enantiomeric excess of about 80%, in excellent agreement with the experimental outcome.

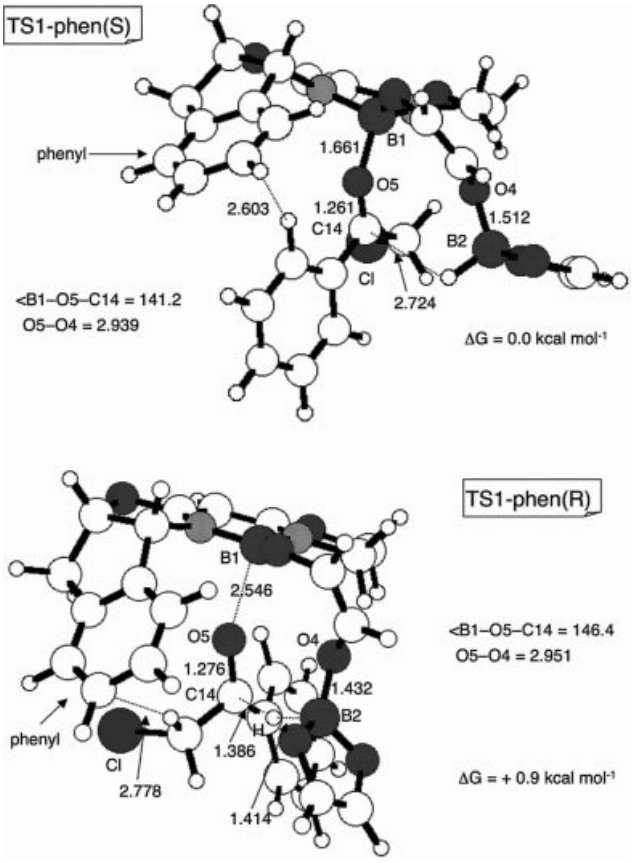

Figure 12. Schematic representation of the structure of the critical points **TS1-phen(S)** and **TS1-phen(R)**, which include the phenyl ring in the model system.

D. Computational Results: the Case of Propyl Phenyl Ketone as a Substrate

To check the reliability of our model in predicting the stereoselectivity of the reaction, we have re-computed the two transition states **TS1(R)** and **TS1(S)** using a model system where the substrate is a propyl phenyl ketone molecule (entry **7b** in Scheme 3). In this case an excess of the stereoisomer with configuration *R* at C14 was experimentally observed (*ee* of 76%).

The two diastereotopic transition states (**TS(R) prop** and **TS(S) prop**) are schematically represented in Figure 13. **TS(R) prop**, i.e. the transition state leading to the product with configuration *R* at C14, is 4.9 kcal mol^{-1} more stable than **TS(S) prop** leading to the opposite configuration. Thus, the prediction of our model, indicating that for the product an excess of the stereoisomer with configuration *R* at C14, is again in agreement with the experimental observation. The key factors that determine the lower activation energy of **TS(R) prop** with respect to **TS(S) prop** are similar to those discussed in the previous section. The stabilizing B1–O5 interaction is stronger in the former case than in the latter (the B1–O5 distance is 1.643 Å in **TS(R) prop** and 1.664 Å in **TS(S) prop**), while the O5–O4 repulsion has the opposite trend as indicated by the O5–O4 distance (2.940 and 2.879 Å in **TS(R) prop** and **TS(S) prop**, respectively). Once again the planar phenyl ring plays a key role in allowing a shorter B1–O5 distance in **TS(R) prop** without increasing the O5–O4 repulsion too much and the repulsion between the phenyl ring itself and the unsaturated five-membered cycle of the B–BOXate moiety.

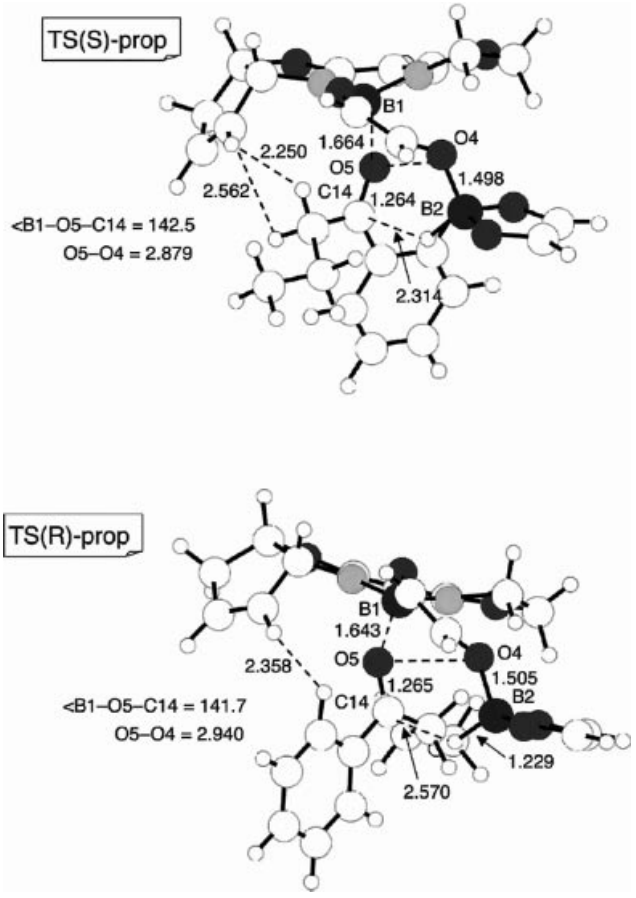

Figure 13. Schematic representation of the structure of the critical points **TS(R)** and **TS(S)** in the case of propyl phenyl ketone as substrate. Some selected geometrical parameters (Å) are reported.

E. Computational Results: The Basis Set Effect

To validate the results obtained with the mixed DZVP/3-21G* basis set, we have carried out single-point computations on the optimized structures using the DZVP basis set on all atoms. These energy values are reported in square brackets in Figure 6. The mechanistic scenario, which stems from these data is identical to that previously discussed. For instance, the barriers for the two transition states **TS1(S)** and **TS1(R)** of the rate-determining step change from 22.7 and 27.0 kcal mol^{-1} to 25.1 and 31.1 kcal mol^{-1}, respectively. Thus, again the pathway leading to the product with config-

 © 2006 Wiley-VCH Verlag GmbH & Co. KGaA, Weinheim

uration S at C14 is favored. Also, the intermediate **M2(S)** and the product **M4** are now 36.0 and 32.0 kcal mol^{-1} below the asymptotic limit, respectively (35.9 and 32.9 kcal mol^{-1} with the less accurate basis). Finally, the barrier for **TS3** varies from 22.6 to 23.3 kcal mol^{-1}.

Conclusions

In this paper the reaction of achiral and chiral bis(oxazolines) (BOX) with catecholborane (CATBH) have been investigated. This reaction provides boron–BOXate complexes that can be used as catalysts in the enantioselective reduction of ketones. The X-ray analysis of two boron–BOXate complexes is in agreement with NMR spectroscopic data and has shown that the chelating bis(oxazoline) ligand forms a six-membered heterocycle when it coordinates the CATBH boron atom. Furthermore, the BOX and the catecholborane skeletons lie on two orthogonal planes with the boron characterized by a tetrahedral coordination geometry. It has been demonstrated that it is possible to achieve good enantiomeric excesses in the reduction of aromatic ketones (*ee* = 72–86%) using a commercially available bis(oxazoline) in the presence of catecholborane.

A DFT investigation has been carried out to shed light on the mechanistic details of the catalytic reduction of aromatic ketones. The most interesting results can be summarized as follows:

(i) The structural features of the B–BOXate complex obtained at the computational level are in good agreement with the experimental outcomes provided by the X-ray analysis.

(ii) The B–BOXate catalyst simultaneously plays different roles. Firstly, it binds the reducing agent CATBH (interaction between the B–BOXate oxygen and the CATBH boron) and causes the weakening of the bond between the boron and the hydrogen that must be transferred as a hydride ion. Secondly, as expected, the boron of the B–BOXate unit interacts with the carbonyl oxygen and makes the prochiral carbon atom more electrophilic. Finally, the repulsions between the side group of the B–BOXate unit (the side unsaturated five-membered ring in our model) and the ketone substituents determine the enantioselectivity of the reaction.

(iii) The transfer of the hydride ion from the boron atom of CATBH to the prochiral carbonyl is the rate-determining step of the catalytic reaction. This transfer can occur on two different pathways involving two diastereotopic transition states, corresponding to the attack of the hydride either onto the *Re* or onto the *Si* face of the ketone. The transition state **TS1(S)** leading to configuration *S* at the new chiral centre (attack onto the *Re* face) in the case of chloroacetophenone has an activation barrier 4.3 kcal mol^{-1} lower than the barrier required by the attack onto the *Si* face [transition state **TS1(R)**]. Thus, our model correctly predicts an excess of the stereoisomer with configuration *S* at the new chiral centre in agreement with the experimental evidence.

(iv) The energy difference between the two diastereotopic transition states, which determines the enantioselectivity of the reaction, is due to complex interplay between the stabilizing B1–O5 interaction (acid–base interaction) involving the B–BOXate boron and the carbonyl oxygen, the repulsion between the ketone carbonyl oxygen and one CATBH oxygen and the repulsion between the side-unsaturated B–BOXate ring and the ketone substituents. This last interaction is particularly important. When the sp^3 carbon (the carbon in an alpha position to the carbonyl in the chloroacetophenone and propyl phenyl ketone) interacts with the B–BOXate ring, the system cannot easily arrange to decrease the repulsive interactions and to increase the boron–oxygen stabilizing effect. This becomes much easier when the configuration at the new chiral centre changes and a phenyl group replaces the sp^3 carbon. In this case, a rotation of the phenyl ring around the carbon–carbon bond can decrease the repulsion and allow a more stabilizing boron–oxygen interaction.

(v) Two possible arrangements of the two reactants (catecholborane and ketone) with respect to the chiral element on the catalyst have been considered. In the preferred arrangement the ketone is close to the chiral element. This minimizes the steric repulsions and the strong acid–base interaction between the B–BOXate boron and the carbonyl oxygen.

(vi) The computation of the free-energy difference between the two transition states **TS1(S)** and **TS1(R)** (4.4 kcal mol^{-1}) corresponds to an enantiomeric excess above 99%, thus much larger than the experimental value (84%). However, when a more realistic model system including a benzene ring, is used, the free-energy difference between the two diastereotopic transition states becomes 0.9 kcal mol^{-1}. This value predicts an enantiomeric excess of about 80%, in very good agreement with the experimental result.

(vii) The role played by the ketone phenyl ring also explains why the reaction is much easier with aromatic than aliphatic ketones. Our analysis indicates that, in the case of aliphatic ketones, it is much more difficult to minimize the repulsions and to increase the stabilizing boron–oxygen interaction and this should make the energy barrier of the rate-determining step larger.

Experimental Section and Computational Details

A) Experimental Section

General Remarks: ^{1}H NMR spectra were recorded using a Varian 200 MHz or a Varian 300 MHz spectrometer. Chemical shifts are reported in ppm relative to tetramethylsilane with the solvent resonance as the internal standard (deuteriochloroform: δ = 7.27 ppm). Data are reported as follows: chemical shifts, multiplicity (s = singlet, d = doublet, t = triplet, q = quartet, br = broad, m = multiplet), coupling constants (Hz). ^{13}C NMR spectra were recorded using a Varian 50 MHz or a Varian 75 MHz spectrometer with complete proton decoupling. Chemical shifts are reported in ppm relative to tetramethylsilane with the solvent as the internal standard (deuteriochloroform: δ = 77.0 ppm). Mass spectra were performed at an ionizing voltage of 70 eV. Chromatographic purification was carried out using 240–400 mesh silica gel. Analytical gas chromatog-

 © 2006 Wiley-VCH Verlag GmbH & Co. KGaA, Weinheim

raphy (GC) was performed using a Hewlett–Packard HP 6890 gas chromatograph with a flame ionization detector and split mode capillary injection system, using a Crosslinked 5% PH ME Siloxane (30 m) column or a Megadex5 chiral (25 m) column. Analytical high performance liquid chromatograph (HPLC) was performed on a HP 1090 liquid chromatograph equipped with a variable wavelength UV detector (deuterium lamp 190–600 nm), using a Daicel Chiralcel™ OD column (0.46 cm I.D.× 25 cm) (Daicel Inc.). HPLC grade 2-propanol and hexane were used as the eluting solvents. Elemental analyses were carried out using a EACE 1110 CHNOS analyzer. All the reactions were carried out in a nitrogen atmosphere in flame-dried glassware using standard inert techniques for introducing reagents and solvents. All ketones were distilled prior to use. All the other commercially obtained reagents were used as received. Neat commercially available catecholborane (Aldrich) stored 5 °C was used for the catalytic reductions. Anhydrous CH_2Cl_2, THF, Et_2O, toluene and CH_3CN were purchased from the Fluka Co.

Preparation of B-Boxate 4: In a oven dried flask anhydrous CH_2Cl_2 (2 mL) was introduced, then achiral BOX **1** ligand (0.05 mmol) and catecholborane(0.75 mmol) were added. The resulting solution was stirred at 25 °C for 3 h then the solvent was evaporated under vacuum. The white solid obtained was washed with anhydrous diethyl ether and collected by filtration (13 mg, yield 86%). ^{1}H NMR (200 MHz, $CDCl_3$): δ = 6.70 (s, 4 H), 4.40 (s, 1 H), 4.16 (s, 4 H), 1.30 (s, 12 H) ppm. ^{13}C NMR (75 MHz, $CDCl_3$): δ = 150.7, 119.1, 109.3, 91.6, 76.4, 62.8, 57.6, 26.3 ppm. ^{11}B (96 MHz, $CDCl_3$): δ = 8.87. IR (Nujol): $\tilde{\nu}$ = 2725, 1558, 1233, 1057, 910, 897 cm^{-1}. $C_{17}H_{21}BN_2O_2$ (296.17): calcd. C 66.22, H 6.45, N 3.29; found: C 66.19, H 6.44, N 3.33.

B-Boxate 5: (25 mg, yield 86%). M. p. 168–171 °C. ^{1}H NMR (300 MHz, $CDCl_3$): δ = 6.99 (m, 24 H), 6.01 (d, 2 H, J = 10.5 Hz), 5.67(d, 2 H, J = 10.5 Hz), 3.91 (s, 1 H) ppm. ^{13}C NMR (75 MHz, $CDCl_3$): δ = 169.5, 150.0, 143.9, 135.5, 133.7, 128.0, 128.9, 127.8, 127.5, 127.4, 126.1, 120.9, 129.1, 118.4, 115.6, 109.4, 108.2, 87.9, 65.2, 57.6 ppm. $[\alpha]_D$ = –165 (χ = 0.69, $CHCl_3$) ppm. $C_{37}H_{29}BN_2O_4$ (576.22): calcd. C77.09, H 5.07, N 4.86; found: C 77.30, H 5.17, N 4.93.

B-Boxate 6: (17 mg, yield 75%). M. p. 158–160 °C. ^{1}H NMR (300 MHz, C_6D_6): δ = 7.94 (d, J = 7.5 Hz, 1 H), 7.60–7.40 (m, 6 H), 7.08–705 (m, 1 H), 6.82 (d, J = 7.5 Hz, 1 H), 6.70 (m, 3 H), 5.29 (s, 1 H), 5.05 (d, 1 H, J = 6.9 Hz), 4.52 (t, J = 6.6 Hz, 1 H), 2.86 (d, J = 9.9 Hz, 1 H), 2.52 (dd, J = 6.6, 9.9 Hz, 1 H) ppm. ^{13}C NMR (75 MHz, C_6D_6): δ = 169.3, 152.3, 144.5, 139.7, 139.5, 129.1, 126.1, 125.6, 121.1, 120.0, 115.7, 109.70, 87.3, 66.8, 57.8, 37.5 ppm. $[\alpha]_D$ = –330 (χ = 0.65, $CHCl_3$). $C_{27}H_{21}BN_2O_4$ (448.16): calcd. C 72.34, H 4.72, N 6.25; found: C 72.47, H 4.81, N 6.28.

General Procedure for the Catalytic Reduction: In an oven dried flask anhydrous CH_2Cl_2 (2 mL) was introduced, then BOX ligand (0.05 mmol) and catecholborane (1 mmol, neat) were added. The resulting solution was stirred at 25 °C for 3 h and then was cooled to 0 °C. The freshly distilled ketone (0.5 mol) was added, then the clear pale yellow solution was stirred at the same temperature for 48 h. The reaction mixture was diluted with Et_2O (5 mL), then NaOH 2 M (5 mL) was carefully added (attention, gas evolution). The two phases were stirred 20–30 min and during this period the aqueous phase turned dark brown. The phases were separated and the aqueous phase extracted with Et_2O (2×3 mL). The organic phase was collected and dried with Na_2SO_4, then purified by chromatography (hexane: Et_2O, 9:1–7:3).

(*R*)-1-Phenylethanol (7a): *ee* = 76%, 49 mg, yield 80%. $[\alpha]_D$ = +36.4 (χ = 2.4, $CHCl_3$). Ref.[20] (*R*)-1-phenylethanol $[\alpha]_D$ = +45.2 (χ = 1.01, CH_2Cl_2). GC analysis: column temperature, 115 °C (isothermal) t_r (major) (*R*)-1-phenylethanol: 12.61 min. t_r (minor) (*S*)-1-phenylethanol: 15.77 min.

(*R*)-1-Phenylpropanol (7b): *ee* = 76%, 44 mg, yield 65%. $[\alpha]_D$ = +28 (χ = 0.8, $CHCl_3$). Ref.[21] (*R*)-1-phenylpropanol $[\alpha]_D$ = +21.5 (χ = 9.3, diethyl ether). GC analysis: column temperature, 110 °C (isothermal) t_r (major) (*R*)-1-phenylpropanol: 25.3 min t_r (minor) (*S*)-1-phenylpropanol: 25.7 min.

(*R*)-3-Methyl-1-phenylbutan-1-ol (7c): *ee* = 74%, 47 mg, yield 57%. $[\alpha]_D$ = +23 (χ = 1.2, $CHCl_3$). Ref.[22] (*R*)-1-phenylbutan-1-ol $[\alpha]_D$ = –39.9 (χ = 0.05, heptane). GC analysis: column temperature, 120 °C (isothermal) t_r (minor) (*S*)-3-methyl-1-phenylbutan-1-ol: 13.8 min. t_r (major) (*R*)-3-methyl-1-phenylbutan-1-ol: 14.1 min.

(*S*)-2-Chloro-1-phenylethanol (7d): *ee* = 84%, 66 mg, yield 85%. $[\alpha]_D$ = +42 (χ = 2.4, $CHCl_3$). Ref.[23] $[\alpha]_D$ = +49.6 (χ = 2.92, cyclohexane). GC analysis: column temperature, 120 °C 20 min, 120 to 230 °C 2 °C/min (program). t_r (major) (*S*)-1-(2′-chloro-1-phenyl)-ethanol: 25.1 min t_r (minor) (*R*)-1-(2′-chloro-1-phenyl)ethanol: 27.6 min.

(*S*)-2-Bromo-1-phenylethanol (7e): *ee* = 86%, 54 mg, yield 54%. $[\alpha]_D$ = +42 (χ = 1.0, $CHCl_3$). Ref.[24] $[\alpha]_D$ = +45.2 (χ = 1.01, CH_2Cl_2). GC analysis: column temperature, 110 °C (isothermal) t_r (minor) (*R*)-1-(2′-bromo-1-phenyl)ethanol: 18.5 min t_r (major) (*S*)-1-(2′-bromo-1-phenyl)ethanol: 19.1 min.

(*R*)-1-Naphthylethanol (7f): *ee* = 72%, 67 mg, yield 78%. $[\alpha]_D$ = +38.5 (χ = 1.06, $CHCl_3$). Ref.[25] (*S*)-1-naphthylethanol $[\alpha]_D$ = –54.8 (χ = 3.34, $CHCl_3$). GC analysis: column temperature, 150 °C (isothermal) t_r (minor) (*S*)-1-naphthylethanol: 27.9 min t_r (major) (*R*)-1-naphthylethanol: 29.15 min.

(*R*)-1-(4′-Chlorophenyl)ethanol (7g): *ee* = 74%, 56 mg, yield 72%. $[\alpha]_D$ = +38.6 (χ = 1.01, $CHCl_3$). Ref.[26] (*S*)-1-(4′-chlorophenyl)ethanol $[\alpha]_D$ = –49.6 (χ = 1.8, Et_2O). GC analysis: column temperature, t_r (major) (*R*)-1-(4′-chlorophenyl)ethanol: 19.9 min t_r (minor) (*S*)-1-(4′-chlorophenyl)ethanol: 25.1 min.

(*R*)-1-(4′-Methylphenyl)ethanol (7h): *ee* = 74%, 44 mg, yield 65%. $[\alpha]_D$ = +28 (χ = 1.0, $CHCl_3$). Ref.[29] (*R*)-1-(4′-methylphenyl)ethanol $[\alpha]_D$ = +35 (χ = 1, $CHCl_3$). GC analysis: column temperature, 115 °C (isothermal) t_r (major) (*R*)-1-(4′-methylphenyl)ethanol: 11.8 min t_r (minor) (*S*)-1-(4′-methylphenyl)ethanol: 15.9 min.

(*R*)-1-(4′-Fluorophenyl)ethanol (7i): *ee* = 81%, 47 mg, yield 67%. $[\alpha]_D$ = +34 (χ = 1.16, $CHCl_3$) Ref.[27] (*S*)-1-(4′-fluorophenyl)ethanol $[\alpha]_D$ = –37.2 (χ = 0.93, MeOH). GC analysis: column temperature, 120 °C (isothermal) t_r (major) (*R*)-1-(4′-fluorophenyl)ethanol: 4.2 min t_r (minor) (*S*)-1-(4′-fluorophenyl)ethanol: 5.5 min.

(*R*)-1-(2′-Bromophenyl)ethanol (7j): *ee* = 57%, 55 mg, yield 55% $[\alpha]_D$ = +27 (χ = 1.08, $CHCl_3$).) Ref.[28] $[\alpha]_D$ = +38.5 (χ = 1.8, $CHCl_3$). GC analysis: column temperature, 120 °C 20 min, 120 to 230 °C 2 °C/min (program). t_r (major) (*S*)-1-(4′-bromophenyl)ethanol: 15.2 min t_r (minor) (*R*)-1-(4′-bromophenyl)ethanol: 16.5 min.

(*S*)-2-Methoxy-1-phenylethanol (7k): *ee* = 58%, 32 mg, yield 42%. $[\alpha]_D$ = +23 (χ = 1.08, $CHCl_3$). Ref.[29] GC analysis: column temperature, 110 °C (isothermal) t_r (major) (*S*)-2-methoxy-1-phenylethanol: 28.0 min t_r (minor) (*R*)-2-methoxy-1-phenylethanol: 30.0 min.

X-ray Crystallographic Study of 4 and 6: The diffraction experiments for **4** and **6** were carried out at room temperature using a Bruker AXS SMART 2000 CCD based diffractometer using graphite-monochromated Mo-K_α radiation (λ = 0.71073 Å). Intensity data were measured over full diffraction spheres using 0.3° wide

 © 2006 Wiley-VCH Verlag GmbH & Co. KGaA, Weinheim

ω scans, crystal-to-detector distance 5.0 cm. The software SMART[30a] was used for collecting frames of data, indexing reflections and determination of lattice parameters. The collected frames were then processed for integration by software SAINT[30a] and an empirical absorption correction was applied with SADABS.[30b] The structures were solved by direct methods (SIR 97)[30c] and subsequent Fourier syntheses and refined by full-matrix least-squares calculations on F^2 (SHELXTL)[31] attributing anisotropic thermal parameters to the non-hydrogen atoms. The aromatic hydrogen atoms were placed in calculated positions and refined with idealized geometry [C(sp^2)–H 0.93 Å] whereas the other H atoms were located in the Fourier map and refined isotropically. Crystal data and details of the data collection for **4** and **6** are reported in Table 1.

CCDC-163357 and -278924 contain the supplementary crystallographic data for this paper. These data can be obtained free of charge from The Cambridge Crystallographic Data Centre via www.ccdc.cam.ac.uk/data_request/cif.

B) Computational Details: All the DFT computations reported here have been performed with the Gaussian 98[32] series of programs using the non-local hybrid Becke's three-parameter exchange functional (denoted as B3LYP in the Gaussian formalism) and locally dense basis sets (LDBS).[33] According to the LDBS approach, in all geometry optimizations the system has been partitioned into two different regions, which were assigned basis sets of different accuracy. One region contains the atoms directly involved in the reaction or in the formation of hydrogen bonds. In this case we have used the DZVP basis, which is a Local Spin Density (LSD)-optimized basis set of double-zeta quality.[34] This basis, which includes polarization functions, is suitable to describe weak hydrogen interactions such as those occurring in the system investigated here. The other region includes all the remaining atoms. For these atoms, contained within the contour line in Figure 4, the 3-21G* basis set[32] has been employed. To obtain more accurate energy values, single-point calculations have been performed using the DZVP basis set on all atoms. The geometry of the various critical points on the reaction surface has been fully optimized with the gradient method available in Gaussian 98. A computation of the harmonic vibrational frequencies has been carried out to determine the nature of each critical point and the ZPE correction has been added to all the energy values.

Supporting Information (see also the footnote on the first page of this article): Calculated transition states for **TS1(S)′** and **TS1(R)′**.

[1] T. P. Yoon, E. N. Jacobsen, *Science* **2003**, *299*, 1691–1693.
[2] A. Pfaltz, *Synlett* **1999**, 835–843.
[3] For recent examples of C_2-bis(oxazoline) Lewis acid complexes as catalysts, see: a) J. S. Johnson, D. A. Evans, *Acc. Chem. Res.* **2000**, *33*, 325–335; b) N. Gathergood, W. Zhuang, K. A. Jørgensen, *J. Am. Chem. Soc.* **2000**, *122*, 12517–12522; c) K. B. Jensen, J. Thorhauge, R. G. Hazell, K. A. Jørgensen, *Angew. Chem. Int. Ed.* **2001**, *40*, 160–163; d) H. Audrain, K. A. Jørgensen, *J. Am. Chem. Soc.* **2000**, *122*, 11543–11544; e) K. Juhl, N. Gathergood, K. A. Jørgensen, *Angew. Chem. Int. Ed.* **2001**, *40*, 2995–2997; f) K. R. Knudsen, T. Risgaard, N. Nishiwaki, K. V. Gothelf, K. A. Jørgensen, *J. Am. Chem. Soc.* **2001**, *123*, 5843–5844; g) N. Nishiwaki, K. R. Knudsen, K. V. Gothelf, K. A. Jørgensen, *Angew. Chem. Int. Ed.* **2001**, *40*, 2992–2995; h) K. Juhl, K. A. Jørgensen, *J. Am. Chem. Soc.* **2002**, *124*, 2420–2421; i) J. Thorhauge, M. Roberson, R. G. Hazell, K. A. Jørgensen, *Chem. Eur. J.* **2002**, *8*, 1888–1898; j) D. A. Evans, M. C. Kozlowski, J. A. Murry, C. S. Burgey, K. R. Campos, B. T. Connell, R. J. Staples, *J. Am. Chem. Soc.* **1999**, *121*, 669–685; k) D. A. Evans, C. S. Burgey, M. C. Kozlowski, S. W. Tregay, *J. Am. Chem. Soc.* **1999**, *121*, 686–699; l) D. A. Evans, K. A. Scheidt, J. N. Johnston, M. C. Willis, *J. Am. Chem. Soc.* **2001**, *123*, 4480–4491; m) D. A. Evans, D. M. Barnes, J. S. Johnson, T. Lectka, P. von Matt, S. J. Miller, J. A. Murry, R. D. Norcross, E. A. Shaughnessy, K. R. Campos, *J. Am. Chem. Soc.* **1999**, *121*, 7582–7594; n) D. A. Evans, S. J. Miller, T. Lectka, P. von Matt, *J. Am. Chem. Soc.* **1999**, *121*, 7559–7573; o) D. A. Evans, T. Rovis, M. C. Kozlowski, J. S. Tedrow, *J. Am. Chem. Soc.* **1999**, *121*, 1994–1995.
[4] M. I. Burguete, J. M. Fraile, J. I. Garcia, E. Garcia-Verdugo, C. I. Herrerias, J. Luis, S. V. A. Mayoral, *J. Org. Chem.* **2001**, *66*, 8893–8901 and references cited therein.
[5] R. Annunziata, M. Benaglia, M. Cinquini, F. Cozzi, M. Pitillo, *J. Org. Chem.* **2001**, *66*, 3160–3166.
[6] a) H. W. Görlitzer, M. Spiegler, R. Arwander, *J. Chem. Soc., Dalton Trans.* **1999**, 4287; b) R. Schumacher, F. Dammast, R. H. U. Reißig, *Chem. Eur. J.* **1997**, *3*, 614–619; c) J. M. Brown, P. J. Guiry, D. W. Price, M. B. Hursthouse, K. Karulov, *Tetrahedron: Asymmetry* **1994**, *5*, 561–564; d) D. Müller, G. Umbricht, B. Weber, A. Pfaltz, *Helv. Chim. Acta* **1991**, *74*, 232–240.
[7] V. Schultze, R. W. Hoffmann, *Chem. Eur. J.* **1999**, *5*, 337–344.
[8] M. Nakamura, A. Hirai, M. Sogi, E. Nakamura, *J. Am. Chem. Soc.* **1998**, *120*, 5846–5847.
[9] R. P. Singh, *Bull. Soc. Chim. Fr.* **1997**, *134*, 765–768.
[10] a) M. Bandini, P. G. Cozzi, L. Negro, A. Umani-Ronchi, *Chem. Commun.* **1999**, 39–40; b) M. Bandini, F. Bernardi, A. Bottoni, P. G. Cozzi, G. P. Miscione, A. Umani-Ronchi, *Eur. J. Org. Chem.* **2003**, 2972–2984.
[11] J. E. Parks, R. H. Holm, *Inorg. Chem.* **1968**, *7*, 1408–1416.
[12] C. E. Radzewich, M. P. Coles, R. F. J. Jordan, *J. Am. Chem. Soc.* **1998**, *120*, 9384–9385.
[13] B. Qian, S. W. Baek, M. R. Smith III, *Polyhedron* **1999**, *18*, 2405–2414.
[14] M. Bandini, P. G. Cozzi, M. Monari, R. Pierciaccante, S. Selva, A. Umani-Ronchi, *Chem. Commun.* **2001**, 1318–1319.
[15] For enantioselective reduction of ketones with boranes see: a) J. Xu, T. Wei, Q. Zhang, *J. Org. Chem.* **2004**, *69*, 6860–6866; b) J. Xu, T. Wei, Q. Zhang, *J. Org. Chem.* **2003**, *68*, 10146–10151; c) N. J. Gilmore, S. Jones, *Tetrahedron: Asymmetry* **2003**, *14*, 2115–2118; d) S. M. Nettles, K. Matos, E. R. Burkhardt, D. R. Rouda, J. A. Corella, *J. Org. Chem.* **2002**, *67*, 2970–2976; e) H. S. Wilkinson, G. J. Tanoury, S. A. Wald, C. H. Senanayake, *Org. Process Res. Dev.* **2002**, *6*, 146–148; f) C. Puigjaner, A. Vidal-Ferran, A. Moyano, M. A. Pericas, A. Riera, *J. Org. Chem.* **1999**, *64*, 7902–7911. For review: see, g) E. J. Corey, C. J. Helal, *Angew. Chem. Int. Ed.* **1998**, *37*, 1986–2012; h) V. A. Glushkov, A. G. Tolstikov, *Russian Chem. Rev.* **2004**, *73*, 581–608; i) M. Wills, J. Hannedouche, *Curr. Opin. Drug Discovery Dev.* **2002**, *5*, 881–891; j) J. M. Brunel, G. Buono, *Top. Curr. Chem.* **2002**, *220* (New Aspects, in: Phosphorus Chemistry I), 79–105; k) M. Wills, M. Gamble, M. Palmer, A. Smith, J. Studley, J. Kenny, *J. Mol. Catal. A* **1999**, *146*, 139–148.
[16] a) G. Alagona, C. Ghio, M. Persico, S. Tomasi, *J. Am. Chem. Soc.* **2003**, *125*, 10027–10039 and references cited therein; b) W. Harb, M. F. Ruiz-López, F. Coutrot, C. Grison, P. Coutrot, *J. Am. Chem. Soc.* **2003**, *126*, 6996–7008 and references cited therein.
[17] V. Stepanenko, M. Ortiz-Marciales, W. Correa, M. De Jesùs, S. Espinosa, L. Ortiz, *Tetrahedron: Asymmetry* **2006**, *17*, 112–115.
[18] S. Dagorne, S. Bellemin-Laponnaz, R. Welter, *Organometallics* **2004**, *23*, 3053–3061.
[19] S. Hong, S. Tian, M. V. Metz, T. J. Marks, *J. Am. Chem. Soc.* **2003**, *125*, 14768–14783.
[20] A. Hashiguchi, K. J. Fujii, K. Haack, T. Matsumura, R. Ikariya, R. Noyori, *Angew. Chem. Int. Ed. Engl.* **1997**, *36*, 288–290.
[21] J. B. Morrison, E. Grandbois, S. I. Howard, *J. Org. Chem.* **1980**, *45*, 4229–4231.

 © 2006 Wiley-VCH Verlag GmbH & Co. KGaA, Weinheim

[22] M. B. Carter, B. Schiott, A. Gutierrez, S. L. Buchwald, *J. Am. Chem. Soc.* **1994**, *116*, 11667–11668.
[23] E. J. Corey, S. Shibata, R. K. Bakshi, *J. Org. Chem.* **1988**, *53*, 2861–2863.
[24] M. Locatelli, P. G. Cozzi, *Angew. Chem. Int. Ed.* **2003**, *42*, 4928–4930.
[25] A. Kohda, K. Nagayoshi, K. Maemoto, T. Sato, *J. Org. Chem.* **1983**, *48*, 425–432.
[26] Y. Kita, Y. Takebe, K. Murata, T. Naka, S. Akai, *J. Org. Chem.* **2000**, *65*, 83–88.
[27] K. Nakamura, T. Matsuda, *J. Org. Chem.* **1998**, *63*, 8957–8964.
[28] J. M. Cherng Fang, T. J. Lu, *J. Org. Chem.* **1999**, *64*, 3207–3212.
[29] M. Bandini, P. G. Cozzi, M. De Angelis, A. Umani-Ronchi, *Tetrahedron Lett.* **2000**, *41*, 1601–1605.
[30] a) *SMART & SAINT* Software Reference Manuals, Version 5.051 (*Windows NT Version*), Bruker Analytical X-ray Instruments Inc.: Madison, Wi, **1998**; b) G. M. Sheldrick, *SADABS*, program for empirical absorption correction, University of Göttingen, Germany, **1996**; c) A. Altomare, M. C. Burla, M. Camalli, G. L. Cascarano, C. Giacovazzo, A. Guagliardi, A. G. G. Moliterni, G. Polidori, R. Spagna, *J. Appl. Crystallogr.* **1999**, *32*, 115–119.
[31] G. M. Sheldrick, SHELXTL*plus* Version 5.1 (*Windows NT version*) *Structure Determination Package*; Bruker Analytical X-ray Instruments Inc.: Madison, WI, **1998**.
[32] M. J. Frisch, G. W. Trucks, H. B. Schlegel, E.G. Scuseria, M. A. Robb, J. R. Cheeseman, V. G. Zakrzewski, J. A. Montgomery, R. E. Stratmann, J. C. Burant, S. Dapprich, J. M. Millam, A. D. Daniels, K. N. Kudin, M. C. Strain, O. Farkas, J. Tomasi, V. Barone, M. Cossi, R. Cammi, B. Mennucci, C. Pomelli, C. Adamo, S. Clifford, J. Ochterski, G. A. Petersson, Q. Cui, K. Morokuma, D. K. Malik, A. D. Rabuck, K. Raghavachari, J. B. Foresman, J. Cioslowski, J. V. Ortiz, B. B. Stefanov, G. Liu, A. Liashenko, P. Piskorz, I. Kamaromi, R. Gomperts, R. L. Martin, D. J. Fox, T. Keith, M. A. Al-Laham, C. Y. Peng, A. Nanayakkara, C. Gonzalez, M. Challacombe, P. M. W. Gill, B. G. Johnson, W. Chen, M. W. Wong, J. L. Andres, C. Gonzalez, M. Head-Gordon, E. S. Replogle, J. A. Pople, *Gaussian 98*, Revision A.6; Gaussian, Inc.: Pittsburgh, PA, **1998**.
[33] a) J. S. Wright, G. A. Di Labio, D. A. Pratt, *Chem. Phys. Lett.* **1998**, *297*, 181–186; b) J. S. Wright, E. R. Johnson, G. A. Di Labio, *J. Am. Chem. Soc.* **2001**, *123*, 1173–1183.
[34] a) N. Godbout, D. R. Salahub, J. Andzelm, E. Wimmer, *Can. J. Chem.* **1992**, *70*, 560–571; b) UniChem. DGauss, Version 2.3.1, **1994**, Cray Research, Inc..

Received: February 15, 2006
Published Online: August 10, 2006

 © 2006 Wiley-VCH Verlag GmbH & Co. KGaA, Weinheim